Li *et al. Journal of Neuroinflammation (2025) 22:11*
https://doi.org/10.1186/s12974-025-03333-6

Journal of Neuroinflammation

RESEARCH

Open Access

Microglial double stranded DNA accumulation induced by DNase II deficiency drives neuroinflammation and neurodegeneration

Ling-jie Li[1,2†], Shi-yu Liang[1,2†], Xiao-ying Sun[1], Jie Zhu[1,2], Xiao-yun Niu[1,3], Xiao-yu Du[1,2], Ya-ru Huang[1*] and Rui-tian Liu[1*]

Abstract

Background Deoxyribonuclease 2 (DNase II) is pivotal in the clearance of cytoplasmic double stranded DNA (dsDNA). Its deficiency incurs DNA accumulation in cytoplasm, which is a hallmark of multiple neurodegenerative diseases. Our previous study showed that neuronal DNase II deficiency drove tau hyperphosphorylation and neurodegeneration (Li et al., Transl Neurodegener 13:39, 2024). Although it has been verified that DNase II participates in type I interferons (IFN-I) mediated autoinflammation and senescence in peripheral systems, the role of microglial DNase II in neuroinflammation and neurodegenerative diseases such as Alzheimer's disease (AD) is still unknown.

Methods The levels of microglial DNase II in triple transgenic AD mice (3xTg-AD) were measured by immunohistochemistry. The cognitive performance of microglial DNase II deficient WT and AD mice was determined using the Morris water maze test, Y-maze test, novel object recognition test and open filed test. To investigate the impact of microglial DNase II deficiency on microglial morphology, cyclic GMP-AMP synthase (cGAS)-stimulator of interferon genes (STING) pathway and IFN-I pathway, neuroinflammation, synapses loss, amyloid pathology and tauopathy, the levels of cGAS-STING and IFN-I pathway related protein, gliosis and proinflammatory cytokines, synaptic protein, complement protein, Aβ levels, phosphorylated tau in the brains of the microglial DNase II deficient WT and AD mice were evaluated by immunolabeling, immunoblotting, q-PCR or ELISA.

Results We found that the levels of DNase II were significantly decreased in the microglia of 3xTg-AD mice. Microglial DNase II deficiency altered microglial morphology and transcriptional signatures, activated the cGAS-STING and IFN-I pathway, initiated neuroinflammation, led to synapse loss via complement-dependent pathway, increased Aβ levels and tauopathy, and induced cognitive decline.

Conclusions Our study shows the effect of microglial DNase II deficiency and cytoplasmic accumulated dsDNA on neuroinflammation, and reveals the initiatory mechanism of AD pathology, suggesting that DNase II is a potential target for neurodegenerative diseases.

†Ling-jie Li and Shi-yu Liang have contributed equally to this work.

*Correspondence:
Ya-ru Huang
yrhuang@ipe.ac.cn
Rui-tian Liu
rtliu@ipe.ac.cn
Full list of author information is available at the end of the article

Keywords DNase II, Alzheimer's disease (AD), cGAS-STING pathway, Type I interferons pathway, Neuroinflammation, Double stranded DNA (dsDNA)

Background

Alzheimer's disease (AD) is a neurodegenerative disease characterized by the extracellular senile plaques formed by β-amyloid (Aβ) and intracellular neurofibrillary tangles consisting of abnormally hyperphosphorylated tau [1, 2]. Accompanying the formation of Aβ plaques and neurofibrillary tangles, the brains of patients with AD are marked by conspicuous and chronic neuroinflammatory responses, manifested by reactive microgliosis, astrogliosis, and elevated levels of proinflammatory cytokines [3, 4]. As resident immune cells in the central nervous system (CNS), microglia play important roles in a variety of physiological homeostasis and pathological occurrence [5–8]. In the early stage of AD, brain microglia play a neuroprotective role [9, 10]. However, as the disease progresses, microglia become overactivated, and the production of proinflammatory cytokines increases, ultimately leading to neuroinflammation and neurotoxicity in AD patients [11]. However, the mechanism by which induces microgliosis remains partially unclear.

DNase II, a member of the deoxyribonuclease family, localized in lysosomes and responsible for the degradation of double-stranded DNA (dsDNA) in cytoplasm, whose downregulation may provoke senescence-associated secretory phenotype (SASP) through the aberrant activation of the cyclic GMP-AMP synthase (cGAS)-stimulator of interferon genes (STING) pathway in senescent cells [12–17]. In previous research, we have identified that DNase II as a potential risk factor of AD, was significantly downregulated in brain of AD patients and AD mouse model [18]. Neuronal DNase II deficiency drove tau hyperphosphorylation by regulating protein kinase and phosphatases, which revealed the initiatory mechanism of tau phosphorylation [18]. Although the physiological and pathological roles of DNase II in peripheral systems and neuron in central nervous system were studied, the roles of DNase II in microglia are relatively poorly understood.

The activation of cGAS-STING pathway induced by cytoplasmic dsDNA has emerged as a critical mechanism for coupling the sensing of DNA to the induction of powerful innate immune defense programs, which also is a major driver of inflammatory diseases [19]. Recent studies have demonstrated an involvement of the activated cGAS-STING pathway induced by dsDNA in several neurological disorders such as ischemic brain injury [20], Parkinson disease [21], Huntington disease [22] and amyotrophic lateral sclerosis [23]. In particular, the microglial cGAS-STING and IFN-I pathway activated by dsDNA likely to play an important role in brain inflammation of AD [24–29]. Nevertheless, the mechanism of dsDNA accumulation in microglia remains elusive. We here found that the levels of DNase II in microglia of 3xTg-AD mice were significantly decreased. We consequently speculate that microglial DNase II plays an important role in the development of AD neuropathology by inducing dsDNA accumulation in cytoplasm.

In this study, we established microglial DNase II knockdown models in vitro and in vivo, and explored the effect of microglial DNase II on microglial transcriptional signatures and function, cGAS-STING pathway and IFN-I pathway dependent neuroinflammation, synapse loss, complement pathway, Aβ level, tauopathy and cognition. Our results reveal a previously unknown role of the microglial DNase II in neuroinflammation and neurodegeneration in AD.

Materials and methods

Animals and treatment

Tmem119^{CreERT2} mice were originally obtained from Jackson Laboratory (Stock No: 031820). 3xTg-AD mice with 3 muted genes, *Psen1*、*APPSwe*、*tauP301L* were purchased from Beijing HFK Bioscience Co., Ltd. (Beijing, China). *Tmem119*^{CreERT2} and 3xTg-AD mice in a C57BL/6 background were housed in our specific pathogen-free (SPF) animal facility. Homozygous *Tmem119*^{CreERT2} mice and homozygous 3xTg-AD transgenic knock-in mice were crossed to obtain the *Tmem119*^{CreERT2}/3xTg-AD genotype. Homozygous colonies were maintained.

All mice for experiments were group-housed, provided food and water ad libitum, and kept in a colony room at 22 ± 2 °C and 45% ± 10% humidity on a reverse 12 h light/dark cycle. All animal experiments were performed in accordance with the China Public Health Service Guide for the Care and Use of Laboratory Animals. Experiments involving mice and protocols were approved by the Institutional Animal Care and Use Committee of Tsinghua University.

5-month-old male homozygous *Tmem119*^{CreERT2} mice (hereafter referred to as WT mice) or 5-month-old male homozygous *Tmem119*^{CreERT2}/3xTg-AD mice (hereafter referred to as AD mice) were divided into two groups

(n = 7–8 mice per group), injected with AAV-shDNase2a (WT-KD or 3xTg-KD) or AAV-shCON virus (WT-CON or 3xTg-CON), respectively.

Primary microglia culture

Primary microglia were obtained from mixed glia cultured as previously described [30]. Briefly, hippocampi were isolated and homogenized into single-cell suspensions by triturating with fire-polished Pasteur pipettes in Dulbecco's modified Eagle's medium (DMEM, Gibco, #11965-092) containing 0.5% penicillin/streptomycin (Gibco, #15070063), GlutaMAX (Gibco, #35050061), and heat-inactivated 10% fetal bovine serum (FBS, Gibco, #10099141). Homogenized tissues were plated at 75 cm^2 T-flask and incubated for 2 weeks. Floating microglia were detached from flasks by mild shaking and then filtered through a 70-μm cell strainer to remove cell clumps or debris. Microglia were plated onto culture dishes at an appropriate density.

Cell culture

293 T cells were purchased from ATCC (CRL-3216) and were cultured in DMEM medium (Gibco, #C11965500CP) supplemented with 10% fetal bovine serum (FBS) (Gibco, #10099141), and 0.5% penicillin and streptomycin in 5% CO_2 at 37 °C.

Lentivirus production and infection

All shRNAs were chemically synthesized from Invitrogen and inserted into the pSicoR (Addgene). Lentiviral package plasmids (Addgene) and the pSicoR were transfected into 293 T cells by Zlip2000 (Beijing Zoman biotechnology, #ZC302-2) according to the instructions. The supernatant containing lentivirus was collected at 48 h after transfection and centrifuged at 3000 rpm for 5 min to remove the cell debris and further ultracentrifuged to obtain high-titer stocks. The pellet was resuspended in PBS and stored at −80 °C. The final viral concentration was calculated by q-PCR assay. The shRNA sequence is as follows: shDNase2a, 5′-GGGTCTAGGGATACTCCAAAG-3′; shCON, 5′-GAAGTCGTGAGAAGTAGAA-3′.

Stereotaxic injection of AAV

MG1.2 subtype of AAV viruses purchased from Obio Technology (Shanghai, China) encoding pAAV-CBG-DIO-EGFP-miR30shRNA (Scramble)-WPRE and pAAV-CBG-DIO-EGFP-miR30shRNA (DNase2a)-WPRE were injected into *Tmem119*^{CreERT2} and *Tmem119*^{CreERT2}/3xTg AD mice to induce microglia specific DNase2a knockdown. The effective interference sequence of mouse DNase2a shRNA in AAV-DNase2a shRNA was 5′-GGG TCTAGGGATACTCCAAAG-3′. Scramble sequence used to construct a nontargeting control virus was 5′-GAAGTCGTGAGAAGTAGAA-3′. These virus titers were $1–2\times10^{13}$ vg/ml. We divided the viral vector into aliquots and stored it at −80 °C until use.

Stereotactic surgery was performed to deliver the AAV vector. Briefly, mice were deeply anesthetized with a mixture of ketamine (100 mg/kg) and xylazine (10 mg/kg). The target coordinates were as follows: anteroposterior (AP) = −2.06 mm, mediolateral (ML) = ± 1.5 mm, dorsoventral (DV) = −1.5 mm (CA1)/−2 mm (DG) from bregma (Fig. S1B).

To knockdown microglial DNase II, 5-month-old WT mice and 5-month-old AD mice were performed craniotomy around the target mark and received 2 μL ($1–2\times10^{13}$ vg/mL) of AAV-shDNase2a or AAV-shCON by bilaterally injection. The rate of injection was 0.5 μL/min and the needle stayed in place for additional 5 min after injection for absorption completely. After surgery, the surgical site was cleaned with sterile saline and the incision was sutured. All mice were monitored and post-surgical care was provided. 4 weeks after, mice were performed behavioral tests, and then sacrificed for biochemical and histological analysis.

Tamoxifen administration

Tamoxifen (Sigma-Aldrich, T5648) was dissolved in corn oil at 20 mg/ml under agitation for several hours in the dark and kept at room temperature for 2–3 d. Tamoxifen was injected (i.p., 100 mg kg^{-1}) for 5 consecutive days after virus injection.

Morris water maze (MWM) test

The MWM test was performed as described previously with minor modifications [31]. Briefly, the water maze consisted of a pool (120 cm in diameter) with opaque water (22 ± 1 °C) and a platform (10 cm in diameter) submerged 1.0 cm under the water. In the training phase (days 1–5) mice were allowed to swim for 60 s to find the platform, on which they were allowed to stay for 20 s. Mice unable to locate the platform were guided to it. All mice were trained twice a day over five consecutive days, with an interval of 3–4 h. 24 h after the last training trial, the mice were tested for memory retention in a probe trial in the absence of the platform. The duration of the probe trial was 60 s. The swimming activity of each mouse was recorded through the video camera (Sony, Tokyo, Japan).

Forced Y-maze test

Y-maze is made up of three identical arms (8 cm × 30 cm × 15 cm) covered with black paper and

separated by an angle of 120°.The test consisted of 2 trials separated by an interval of 1 h. For the training trial, each mouse was allowed to explore freely only 2 arms (the start and familiar arms) of the maze for 10 min, and the third arm (the new arm) was blocked. For the testing trial, the mice were put back in the same starting arm as in training trial with free access to all three arms for 5 min. All trials were recorded by a video system, and the number of entries and time spent in each arm were analyzed. The arms were cleaned with 75% ethanol solution between trials.

Spontaneous Y-maze test

The spontaneous Y-maze test aims to assess short-term memory performance. The maze was the same as the forced Y-maze, except that the marker at the end of each arm was changed to eliminate the effects of the former forced Y-maze. This test consisted of a single 5 min trial in which the mouse was allowed to move freely to all three arms of the Y-maze. The series of arm entries, including possible returns into the same arm, was recorded with a camera connected to a computer. An alternation was defined as entry into all three arms on consecutive occasions. The number of maximum alternations was therefore the total number of arm entries minus 2, and the percentage of alternations was calculated as (actual alternations/maximum alternations) × 100%.

Novel object recognition (NOR) test

Briefly, in the habituation phase, each mouse was allowed freely explore the behavioral arena (50 cm × 50 cm × 25 cm white plastic box, empty) for 5 min 1 day before testing; For the training session, mice were placed in the box having two identical objects in the upper two corners and allowed to explore for 5 min. After a 6 h interval, mice were allowed to explore one familiar and one novel object for 5 min in the same box in the test session. The time spent exploring and sniffing each object was recorded. The results were expressed as the discrimination index, which refers to: $(Time_{novel} - Time_{old}) / (Time_{novel} + Time_{old})$. The box was cleaned with 75% alcohol between trials to eliminate olfactory cues.

Open field test

Mice were placed individually in the center of the chamber ($27 \times 27 \times 20.3$ cm^3) equipped with a camera (Sony, Tokyo, Japan). Their free behavior was recorded for 10 min. Velocity, center duration and total distance were quantitatively analyzed. Chamber was cleaned with 75% ethanol between trials.

Immunocytochemistry (ICC)

Cells were washed with PBS three times, fixed in 4% paraformaldehyde (PFA) for 20 min at room temperature and permeabilized with 0.3% Triton X-100 for 30 min and blocked with 10% donkey serum albumin (DSA) in PBS for 1 h at room temperature. Then cells were incubated with primary antibodies overnight at 4 °C, followed by corresponding fluorescently-conjugated (-488, -594 or -647) secondary antibodies for 45 min and counterstained with DAPI (1:10,000) for 15 min at room temperature in dark, and then mounted on coverslips with anti-fade mounting medium. Fluorescence signals were captured on a laser scanning confocal microscope (Leica TCS SP8, Germany).

Immunohistochemistry (IHC)

Mice were deeply anesthetized and perfused with ice-cold PBS containing heparin (10 U/mL) before sacrificed. Mouse brains were immediately removed and divided along the sagittal plane. The left brain hemisphere was fixed in 4% PFA at 4 °C overnight and processed for paraffin-embedded sections. For immunohistochemistry analysis, 5 μm or 15 μm coronal paraffin-embedded serial sections were deparaffinized and subjected to antigen retrieval using citrate buffer (0.01 M, pH 6.0, 0.05% Tween-20) at 95 °C for 20 min. The sections were then incubated with 0.3% H_2O_2 and washed 3 times with 1 × PBS. Sections were then permeabilized and blocked with 10% goat serum albumin (GSA) or donkey serum albumin (DSA) in 0.3% Triton-X 100 for 1 h at room temperature. Then sections were incubated with the primary antibodies overnight at 4 °C, followed by corresponding secondary antibodies conjugated to Alexa Fluor 488, -594 or -647, respectively. The sections were imaged on the Leica TCS SP8 confocal microscope. For 3′-Diaminobenzidine (DAB) immunostaining, the sections were incubated with a corresponding HRP-labeled secondary antibody and visualized with DAB by an Olympus IX73 inverted microscope with DP80 camera. All images were analyzed by Image J software.

The following primary antibodies were used for IHC and ICC assay in this study: anti-MAP2 antibody (Invitrogen, #PA1-16751, 1:500), anti-NeuN antibody (Abcam, #ab104224, 1:100), anti-IBA1 antibody (Genetex, #GTX101495, 1:200), anti-IBA1 antibody (Abcam, #ab283319, 1:100), anti-IBA1 antibody (Abcam, #ab5076, 1:100), anti-GFAP antibody (Cell Signaling Technology, #3670S, 1:200), anti-DNase II antibody (Proteintech, #15934-1-AP, 1:200), anti-PSD95 antibody (Abcam, #ab13552, 1:200), anti-synaptophysin antibody (Abcam, #ab32127, 1:500), anti-phospho-tau (Ser202, Thr205) (Invitrogen, #MN1020, 1:200), anti-GFP (Abcam, #ab1218, 1:200), anti-C3 (Abcam, #ab200999,

1:200), anti-dsDNA marker (Santa cruz biotechnology, #SC-58749, 1:50), anti-γH2AX (phospho S139) (Abcam, #ab81299, 1:250), anti-phospho-STAT1 (Abcam, #ab29045, 1:100).

The following secondary antibodies were used for IHC and ICC assay in this study: Donkey anti-Mouse IgG H&L (Alexa Fluor® 488) (Abcam, #ab150105, 1:500), Donkey anti-Mouse IgG H&L (Alexa Fluor® 555) (Abcam, #ab150110, 1: 500), Donkey anti-Rabbit IgG H&L (Alexa Fluor® 488) (Abcam, #ab150073, 1: 500), Donkey anti-Rabbit IgG H&L (Alexa Fluor® 647) (Abcam, #ab150063, 1: 500), Donkey anti-Goat IgG H&L (Alexa Fluor® 555) (Abcam, #ab150130, 1: 500), Donkey anti-Chicken IgY (H + L) (Alexa Fluor® 488) (Yeasen, #34606ES60, 1: 500), Donkey anti-Chicken IgY (H + L) (Alexa Fluor® 594) (Yeasen, #34612ES60, 1: 500), Goat anti-Mouse IgG (HRP) (Abcam, #ab6789, 1: 300), Goat anti-Rabbit IgG (HRP) (Abcam, #ab6721, 1: 300).

RNA extraction and quantitative PCR (q-PCR)

Total RNA from cell lysates was extracted using TRIzol reagent. Reverse transcription was performed by EasyQuick RT MasterMix (Cwbio, #CW2019M) according to the manufacturer's instructions. Relative gene expression of the cDNA was detected by real-time q-PCR using the 7500 Fast Real-Time PCR System (Applied Biosystems) and SYBR Select Master Mix (Applied Biosystems, #4472908). Expression levels of the target genes were normalized to β-actin. The primer sequences used in this study were described in Table S1.

Brain lysate preparation

The mouse hippocampus tissues were homogenized in RIPA lysis buffer (MedChemExpress, #HY-K1001) containing phosphatase inhibitor cocktails (Solarbio Left Sciences, #P1260) and protease inhibitor cocktail set I (Millipore, #539131) using Tissue LyserII (QIAGEN) and then centrifuged at 15,000×*g* for 30 min at 4 °C to collect the supernatant (RIPA-soluble fraction). The pellets were resuspended in guanidine buffer (5.0 M guanidine-HCl/50 mM Tris–HCl, pH 8.0) and centrifuged at 15,000×*g* for 1 h at 4 °C to obtain supernatants containing insoluble proteins (RIPA-insoluble fraction). The protein concentrations of soluble and insoluble fractions were determined using the BCA protein assay (Thermo Fisher Scientific, #23225) according to the manufacturer's instructions.

Western blots

Protein samples from mouse hippocampus tissues or cell lysates were separated using 10–12% SDS-PAGE gels (Invitrogen) and transferred onto nitrocellulose membranes (Merck Millipore). After blocking with 5% non-fat milk for 1 h at room temperature, the membrane was incubated with the corresponding primary antibodies overnight at 4 °C. Then HRP-conjugated secondary antibodies were applied at a concentration of 1:5000 for 1 h at room temperature. The bands in immunoblots were visualized by enhanced chemiluminescence using an Amersham imager 680 imaging system (GE Healthcare) and quantified by densitometry and Image J software.

The following primary antibodies were used for Western blots assay in this study: Anti-β-actin (Abcam, #ab8226, 1:1000), anti-DNase II (Proteintech, #15934-1-AP, 1:500), anti-γH2AX (phospho S139) (Abcam, #ab81299, 1:1000), anti-phospho-tau (Ser202, Thr205) (Invitrogen, #MN1020, 1:500), anti-OC (Millipore, #AB2286, 1:1000), anti-PSD95 (Abcam, #ab238135, 1:1000), anti-synaptophysin (Abcam, #ab32127, 1:1000), anti-phospho-TBK1/NAK (Ser172) (Cell Signaling Technology, #5483, 1:1000), anti-TBK1 (Abcam, #ab40676, 1:1000), anti-GFAP (Cell Signaling Technology, #3670S, 1:1000), anti-IBA1 (Abcam, #ab283319, 1:1000), anti-STING (Beyotime, #AG5348, 1:1000), anti-phospho-STING (Affinity, #AF7416, 1:1000), anti-cGAS (Abcam, #ab302617, 1:1000), anti-phospho-STAT1 (Abcam, #ab29045, 1:1000), anti-IRF3 (Beyotime, #AF2485, 1:1000), anti-phospho-IRF3 (Ser396) (Cell Signaling Technology, #29047, 1:1000), anti-c-Fos (Abcam, #ab222699, 1:1000), anti-C1q (Invitrogen, #MA1-40311, 1:50) anti-C3 (Abcam, #ab200999, 1:1000), anti-APP antibody (Abcam, #ab32136, 1:1000), anti-PS1 antibody (Abcam, #ab76083, 1:1000), anti-BACE1 antibody (Abcam, #ab183612, 1:1000).

The following secondary antibodies were used for Western blots assay in this study: Goat anti-Rabbit IgG (HRP) (Abcam, #ab6721, 1:10000), Goat anti-Mouse IgG (HRP) (Abcam, #ab6789, 1:10000).

Dot-blot

One microgram (0.5 μg/μL) of the brain lysates was applied to nitrocellulose membranes. The membrane was blocked with 5% non-fat milk in TBST and incubated with OC (Millipore, #AB2286, 1:1000) or anti-β-actin (Abcam, #ab8226, 1:1000) antibodies for 1 h at room temperature, followed by appropriate HPR-conjugated secondary antibodies. Immunoreactive blots were developed with Super-Signal West Pico Plus Chemiluminescent Substrate kit (Pierce, UB278521), and quantified by densitometry using ImageJ software (NIH).

Measurement of IL-6, IL-1β and TNF-α

The levels of IL-6, IL-1β, and TNF-α in the brain lysates of mice or the supernatant of primary microglia were determined using corresponding ELISA kits (Biolegend, #431304 for IL-6; #432601 for IL-1β; #430904 for TNF-α) according to the manufacturer's protocols. A SpectraMax M5 microplate reader (Molecular Devices, Sunnyvale, CA) was used to measure the absorbance at 450 nm.

Measurement of Aβ40 and Aβ42

The levels of Aβ40 and Aβ42 in the insoluble hippocampus lysates of mice were determined using Aβ peptide panel 1 kit (4G8) (Meso Scale Diagnostics, #K15199E) according to the instructions. Briefly, 25 µL of mouse brain homogenates and 25 µL detection antibody were added to the plate, and the plate was incubated at room temperature for 2 h with shaking at 500 rpm. Washing plate for 4 times, after adding the read buffer, the Aβ40 and Aβ42 levels were measured by the MSD-S600 reader.

Statistical analysis

Statistical testing was performed using Prism (GraphPad Software). For comparisons between groups, first, it was determined whether the data were normally distributed using the Shapiro–Wilk test (Sigma-Plot). If data were normally distributed, one-way or two-way ANOVA was used with Tukey's test for pairwise comparisons or an unpaired *t* test with two-tailed p values. If not, Mann–Whitney test (two groups) or Kruskal–Wallis one-way ANOVA on ranks (three or more groups) with Two-stage step-up method Benjamini, Krieger and Yekutieli test was used. Results were expressed as group mean ± SEM, and $P < 0.05$ was considered statistically significant. $^{*}P < 0.05$, $^{**}P < 0.01$, $^{***}P < 0.001$, $^{****}P < 0.0001$, ns, not significant.

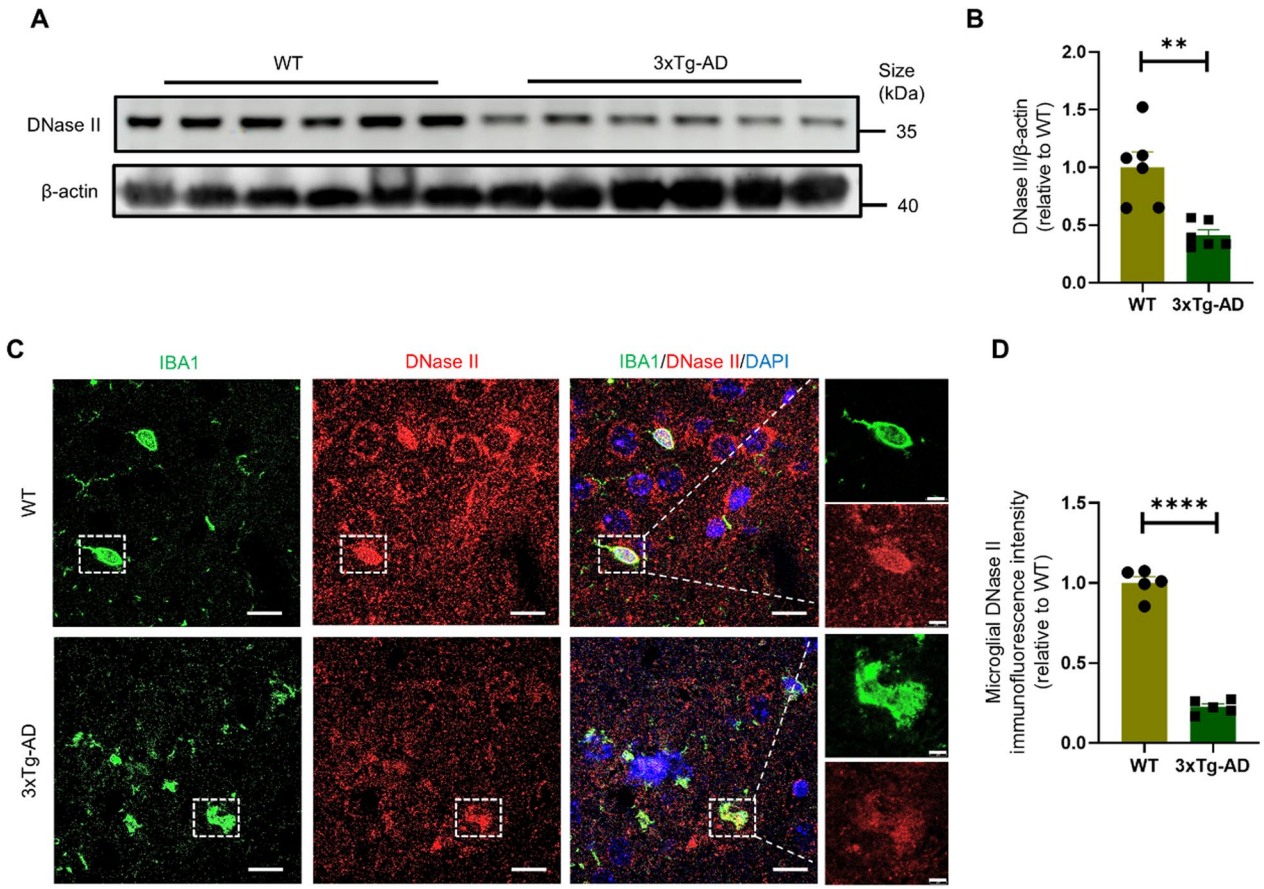

Fig. 1 The levels of microglial DNase II are decreased in the brains of AD model mice. **A** Western blots analysis of DNase II in the hippocampus lysates of 6-month-old WT mice and 3xTg-AD mice. **B** Quantitation of the levels of DNase II in (**A**). n = 6 mice per group. **C** Representative images of DNase II (red) and IBA1 (green) fluorescence staining in the hippocampus of 6-month-old WT mice and 3xTg-AD mice. Scale bars, 25 µm (left) and 5 µm (right). **D** Quantification of DNase II immunofluorescence intensity in (**C**). n = 5 mice per group. Data are mean ± SEM, and an unpaired *t* test with two-tailed was used for statistical analysis. $^{*}P < 0.05$, $^{**}P < 0.01$, $^{***}P < 0.001$, $^{****}P < 0.0001$, ns, not significant

Results

The levels of microglial DNase II are decreased in the brains of AD model mice

To confirm the levels of DNase II in AD model mice, we measured DNase II protein in the hippocampus lysates of 6-month-old 3xTg-AD mice. Compared with 6-month-old WT mice, 3xTg-AD mice showed significantly decreased levels of DNase II in their hippocampi (Fig. 1A, B). Moreover, our immunohistochemistry (IHC) results further showed that DNase II levels in microglia of 3xTg-AD mice were consistently lower than that of 6-month-old WT mice. (Fig. 1C, D).

Microglial DNase II deficiency induces cognitive impairment in WT and AD mice

To examine the role of microglial DNase II in the development of AD neuropathology, we generated Cre-inducible AAV to knockdown the expression of microglial DNase II (Fig. S1A). Our AAV-DIO carries the inverted genes of shDNase2a and EGFP which were flanked by two types of lox sequences, loxP and lox2722 (Fig. S1A), which expressed the floxed genes if Cre was present. In this study, spatial specificity of DNase II knockdown was achieved by stereotaxic injection of AAV to cornu ammonis 1 (CA1) and dentate gyrus (DG) of the dorsal hippocampi cell type-specific Cre mouse lines, 5-month-old *Tmem119*^{CreERT2} mice (hereafter referred to as WT mice) and *Tmem119*^{CreERT2}/3xTg-AD transgenic mice (hereafter referred to as AD mice) (Fig. S1B). The treated mice selectively expressed the tamoxifen-inducible Cre recombinase in microglia for selective knockdown of microglial DNase II. We firstly examined the AAV expression in the brains by observing the green fluorescent protein (GFP)-expressing microglia four weeks post injection. The GFP was widely expressed in microglia in the mice injected with AAV-shDNase2a or AAV-CON (Fig. S1C). We next examined the damaged DNA by immunolabeling of γH2AX, a marker of dsDNA breaks. The results showed that the immunoreactivity of γH2AX was significantly increased in the microglia treated by AAV-shDNase2a, indicating that dsDNA accumulated in corresponding microglia (Fig. S1D and S1E). Additionally, our western blots showed that the expression of DNase II was significantly decreased in the mice treated with AAV-shDNase2a (Fig. S1F and S1G).

Mice were then subjected to forced Y-maze, spontaneous Y-maze, open field, novel object recognition (NOR) and Morris water maze (MWM) tests to evaluate their memory and cognition (Fig. 2A). No significant difference in mouse motor function was observed in any experimental groups of the WT and AD mice (Fig. S2A–C). As shown, WT mice injected with AAV-shDNase2a exhibited reduced residence time (Fig. 2B) and number of entries (Fig. 2C) in the novel arm in forced Y-maze test (Fig. S2D) and less alternation (Fig. 2D) in the spontaneous Y-maze test compared with WT-CON mice, indicating that decreased DNase II in microglia induced the deficits in both working memory and short-term reference memory retrieval. Similarly, 3xTg-KD mice showed more severe deficits in memory and cognition compared with 3xTg-CON mice (Figs. 2B–D and S2D). In the open field test, WT and AD mice injected with AAV-shDNase2a traveled less distances (Figs. 2E and S2E) in the central area, suggesting that mice with DNase II knockdown increased anxiety. In NOR test, WT and AD mice injected with AAV-shDNase2a showed decreased discrimination index (Fig. 2F), which further confirmed that microglial DNase II knockdown damaged memory in both WT and AD mice. In MWM training test, WT and AD mice injected with AAV-shDNase2a showed impaired spatial learning ability with longer latency (Fig. 2G). In probe test of MWM, WT-KD mice and 3xTg-KD mice exhibited increased escape latencies (Fig. 2H), fewer platform crossing times (Fig. 2I) compared with their control mice. These results indicated that microglial DNase II knockdown induced remarkable cognitive deficits in WT and AD mice.

Microglial DNase II deficiency activates the cGAS-STING and IFN-I pathway

The cGAS can be activated by cytosolic self-DNA derived from genome [19, 32], and the microglial cGAS-STING and IFN-I pathway is likely to play an important role in the neuropathology of AD patients [24–29]. To determine the effect of microglial DNase II deficiency on cGAS-STING and IFN-I pathway, we first detected microglial phosphorylated STAT1 (p-STAT1), the key marker of IFN-I activation and transcriptional driver of IFN-stimulated genes (ISGs) expression [33]. The levels of p-STAT1 were significantly increased in the microglia in DNase II-deficient WT and AD mice (Fig. 3A, B). Next, we performed western blot to measure the levels of cGAS, stimulator of interferon genes (STING), phosphorylated STING (p-STING) and the downstream mediators of the cGAS-STING cytoplasmic DNA sensing pathway, including TANK-binding kinase 1 (TBK1), phosphorylated TANK-binding kinase 1 (p-TBK1), interferon regulatory factor 3 (IRF3), phosphorylated IRF3 (p-IRF3) and IFN-I pathway protein p-STAT1. The results showed that the levels of cGAS (Fig. 3C, D), p-STING/STING (Fig. 3C, E), p-TBK1/TBK1 (Fig. 3C, F), p-IRF3/IRF3 (Fig. 3C, G), p-STAT1 (Fig. 3C, H) were significantly enhanced in the hippocampus lysates of WT and AD mice treated with AAV-shDNase2a, indicating that microglial DNase II deficiency activated the

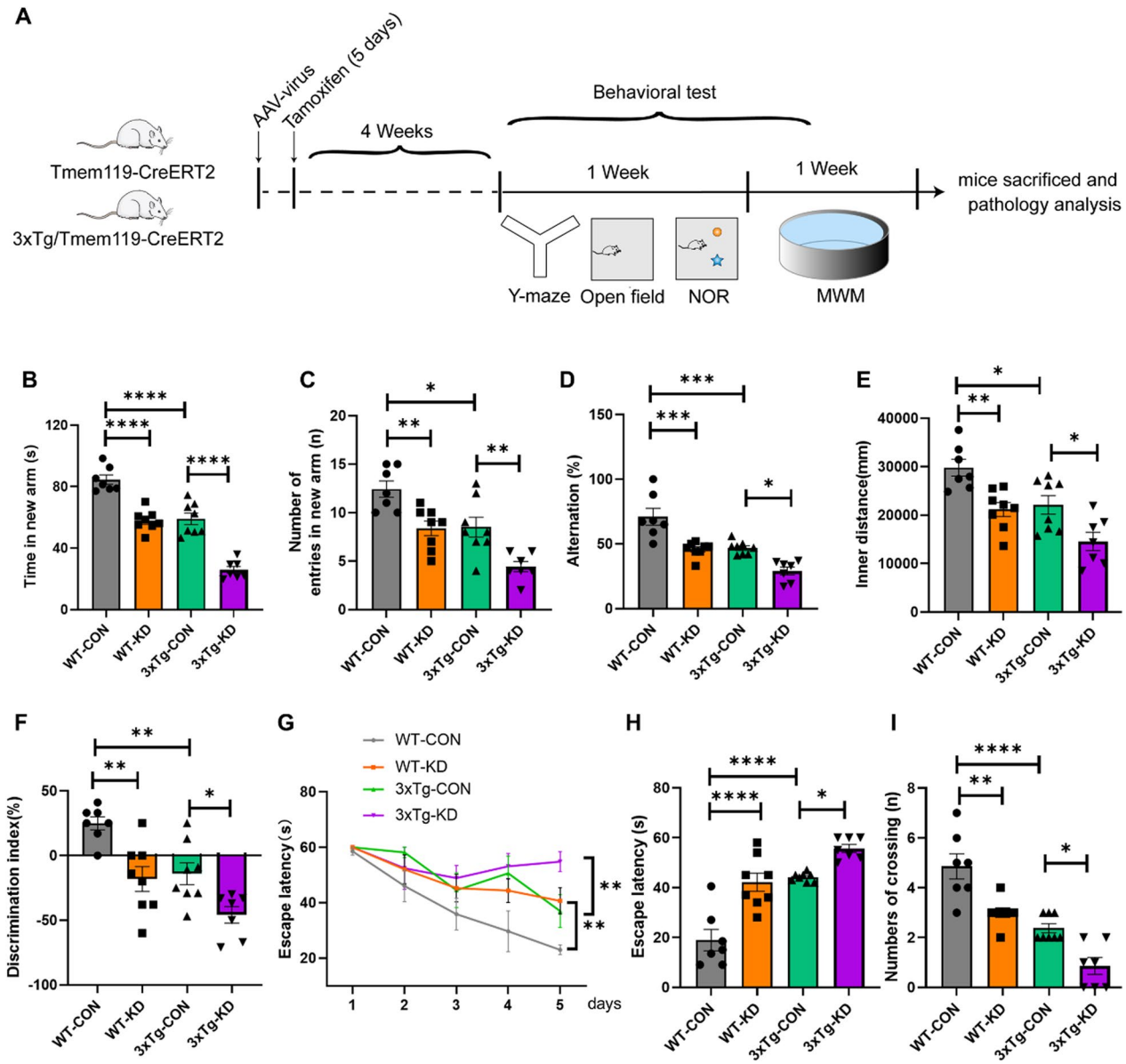

Fig. 2 Microglial DNase II deficiency induces cognitive impairment in WT and AD mice. **A** Schematic representation of the pharmacological treatment and experimental measurement. **B**, **C** The time spent (**B**) and number of entries (**C**) in the novel arm of mice in forced Y-maze. **D** The alternation of mice in a spontaneous Y-maze. **E** The distance traveled of mice in the central area of the open field. **F** Discrimination index of the mice in novel object recognition test. **G** The latency to find the hidden platform during training trials. n = 7–8 mice per group. Data are mean ± SEM, and a two-way ANOVA followed by Tukey's multiple comparison test was used for statistical analysis. **H** The latency to the position of the removed platform during probe trials. **I** The number of platform crossings during probe trials. For (**B**, **D**–**F**, **H**), n = 7–8 mice per group, data are mean ± SEM, and a one-way ANOVA followed by Tukey's multiple comparison test was used for statistical analysis. For (**C**, **I**), n = 7–8 mice per group, data are mean ± SEM, and Kruskal–Wallis one-way ANOVA with two-stage step-up method Benjamini, Krieger, and Yekutieli test was used for statistical analysis. *$P < 0.05$, **$P < 0.01$, ***$P < 0.001$, ****$P < 0.0001$, ns, not significant

cGAS-STING and IFN-I pathway in both WT mice and AD mice.

To further validated the effect of DNase II deficiency on the cGAS-STING and IFN-I pathway in primary microglia, we constructed a lentivirus system carrying *Dnase2a* shRNA (shDNase2a) to knockdown DNase II in primary microglia (Fig. S3). As the results shown, DNase II deficiency significantly increased the levels of γH2AX in microglia (Fig. S3). Then we tested the levels of related proteins of cGAS-STING and IFN-I pathway after reducing DNase II expression. Our western blot

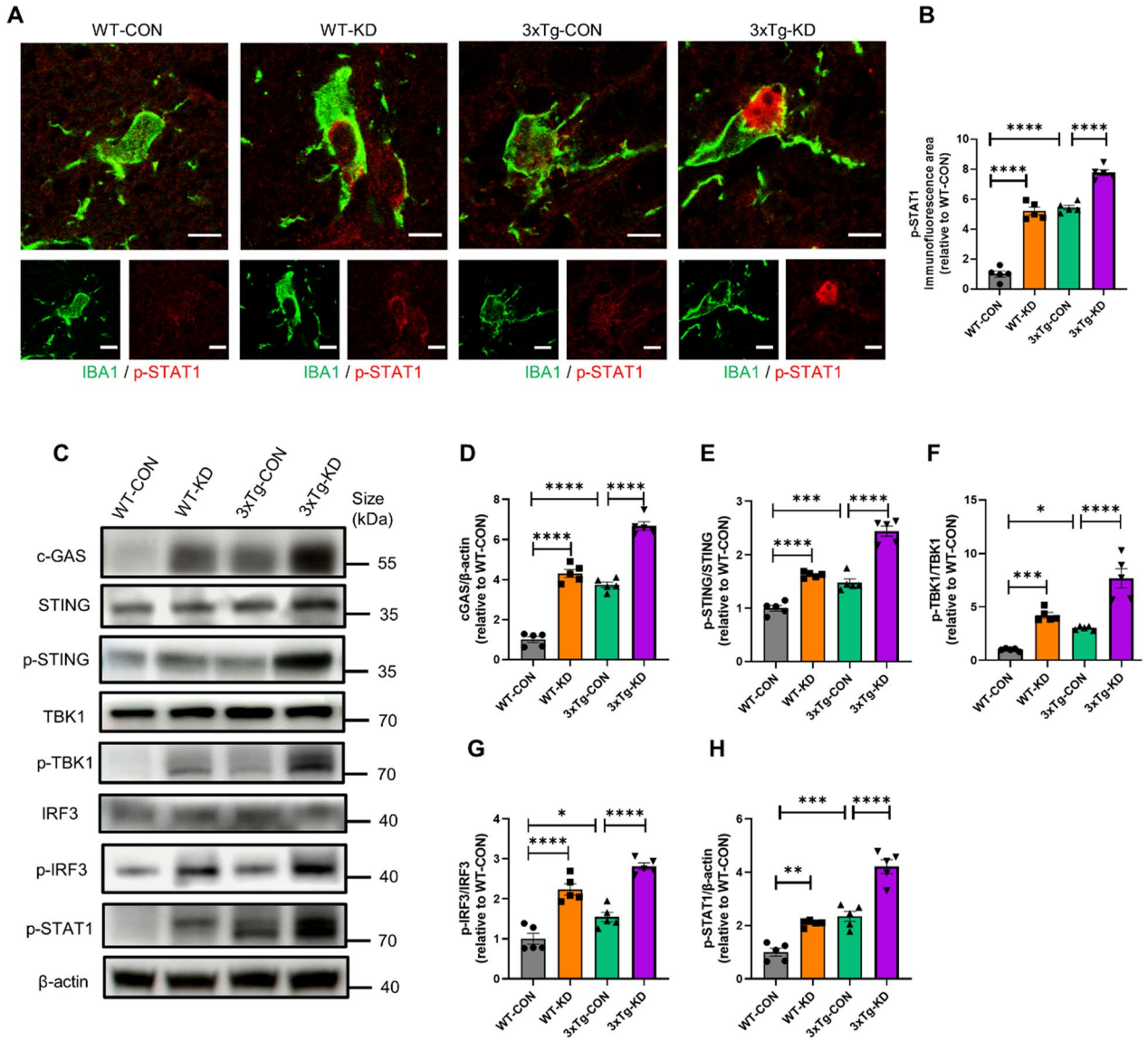

Fig. 3 Microglial DNase II deficiency induces cGAS-STING and I-IFN pathway activation in WT and AD mice. **A** Representative images of p-STAT1 (red) and IBA1 (green) fluorescence staining in the hippocampus of WT mice and AD mice. Scale bars, 5 μm. **B** Quantification of p-STAT1 fluorescent area in (**A**). n = 5 mice per group. **C** Western blots analysis of cGAS, STING, p-STING, TBK1, p-TBK1, IRF3, p-IRF3 and p-STAT1 in the hippocampus lysates of WT mice and AD mice. **D–H** Quantitation of the levels of cGAS (**D**), p-STING/STING (**E**), p-TBK1/TBK1 (**F**), p-IRF3/IRF3 (**G**), p-STAT1 (**H**) in (**C**). For (**D–H**), n = 5 mice per group, data are mean ± SEM, and a one-way ANOVA followed by Tukey's multiple comparison test was used for statistical analysis. **P* < 0.05, ***P* < 0.01, ****P* < 0.001, *****P* < 0.0001, ns, not significant

results showed that the levels of cGAS (Figs. S4A and S4B), p-STING/STING (Figs. S4A and S4C), p-TBK1/TBK1 (Figs. S4A and S4D), p-IRF3/IRF3 (Figs. S4A and S4E), p-STAT1 (Figs. S4A and S4F) were significantly increased in primary microglia. Consistently, as shown by q-PCR analysis, the ISGs including *Isg15*, *Ifitm3*, *Ifit1*, *Igtp*, *Ifit3* and *Irf7* were significantly elevated in the primary microglia infected with shDNase2a (Fig. S4G-K). IRF7 is a master transcriptional regulator of IFN-I response, present increases of *Irf7* level were consistent with previous reports [34, 35]. Our data indicated that microglial DNase II deficiency induced IFN-I response through the cGAS-STING pathway in vivo and in vitro.

DNase II-deficient microglia show altered morphology and transcriptional signatures

Next, we detected the effect of DNase II on the morphology and function of microglia. Compared with

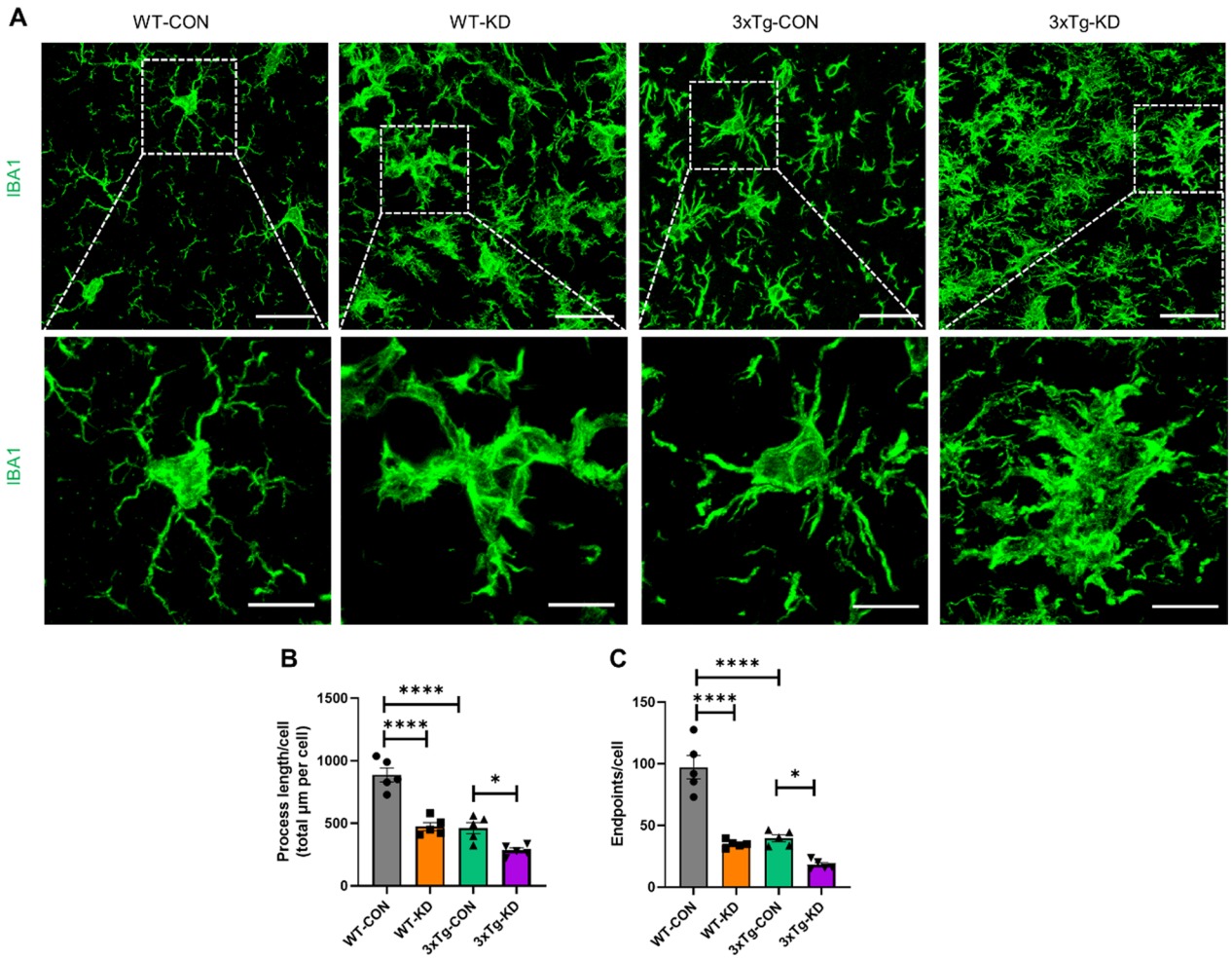

Fig. 4 Microglial DNase II deficiency induces alternation of microglia morphology. **A** Representative images of IBA1 (green)-stained microglial in the brains of WT mice and AD mice. Scale bars, 25 μm (up) and 10 μm (down). **B** Quantification of microglial process length. n = 5 mice per group. **C** Quantification of microglial endpoints. n = 5 mice per group. For (**B**, **C**), data are mean ± SEM, and a one-way ANOVA followed by Tukey's multiple comparison test was used for statistical analysis. *$P < 0.05$, **$P < 0.01$, ***$P < 0.001$, ****$P < 0.0001$, ns, not significant

the microglia in mice that were received AAV-shCON injection, DNase II-deficient microglia in mice that were received AAV-shDNase2a injection increased in their number, and exhibited a reactive morphology with reduced process length and endpoints, while the microglia in 3xTg-KD mice shown higher activation with less process length and endpoints (Fig. 4). Concomitantly, the microglia number in mice that were received AAV-shDNase2a injection also increased, and microglia were more like disease-associated microglia (DAM) displaying a hypertrophic morphology with shorter processes and less endpoints compared with that in mice that were received AAV-shCON injection (Fig. 4A–C).

We further detected the effect of DNase II deficiency on the transcriptional signatures of microglia. The q-PCR results indicated that several M0-homeostatic microglial genes, including *P2ry12, Tmem119, Tgfβr1* and *Cx3cr1* were significantly downregulated in the primary microglia infected with shDNase2a (Fig. S5A). In contrast, several neurodegenerative microglia (MGnD) related genes, including *Apoe, Trem2, Gpnmb and Clec7a* were significantly upregulated in DNase II-deficient primary microglia (Fig. S5B). Moreover, inflammatory cytokine related genes such as *iNOS, IL-6, Tnf-α* and *IL-1β* were induced (Fig. S5C), while the anti-inflammatory cytokine related genes including *Tgfβ, Arg1, IL-4* and *IL-10* were suppressed (Fig. S5D) in DNase II deficient primary microglia. Thus, DNase II deficiency altered microglial morphology and transcriptional signatures.

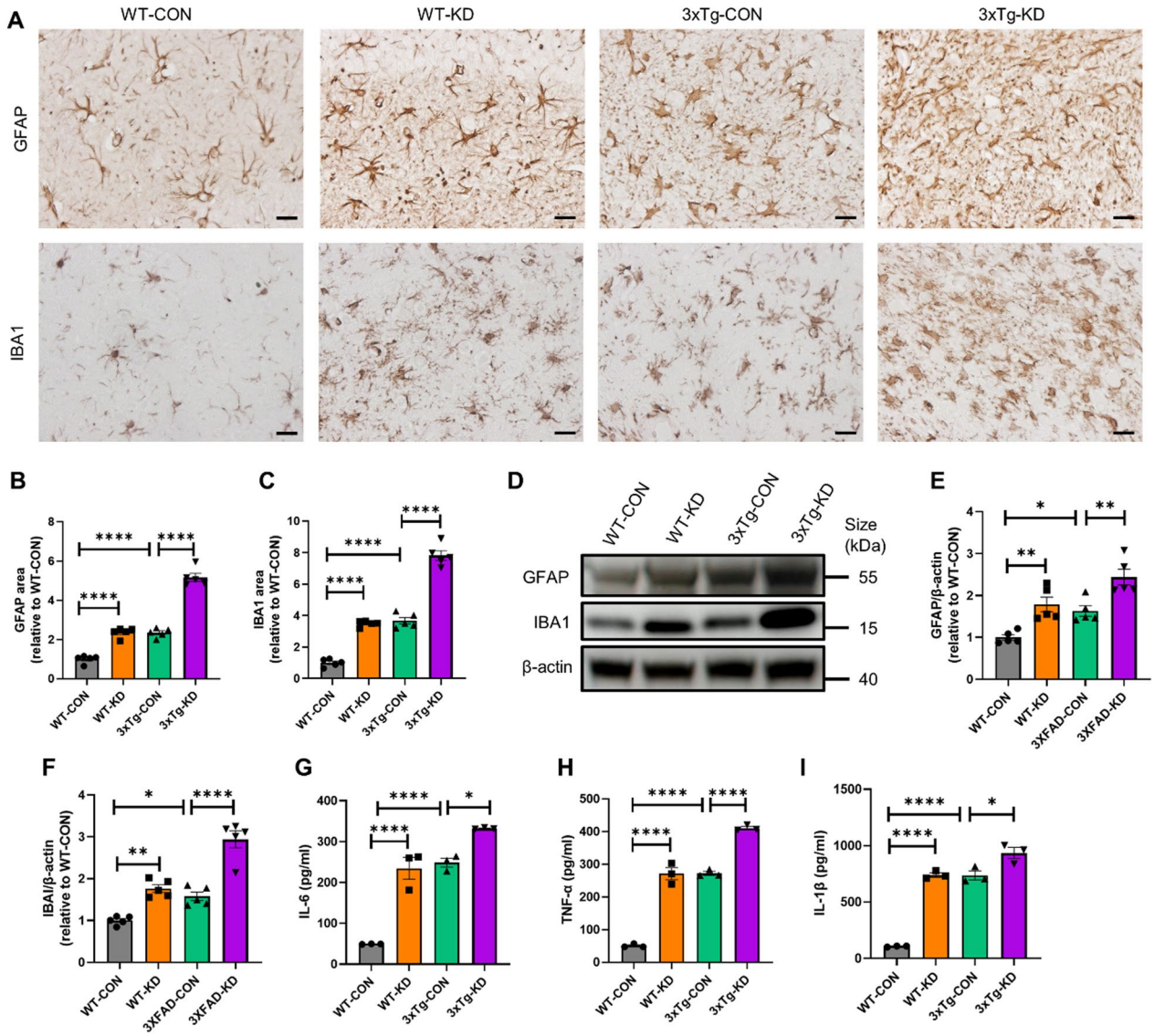

Fig. 5 Microglial DNase II deficiency induces neuroinflammation in WT and AD mice. **A** Detection of astrocytes and microglia by immunolabeling GFAP and IBA1 in the hippocampus of WT mice and AD mice. Scale bars, 20 μm. **B** Quantification of GFAP-labeled area in (**A**). n = 5 mice per group. **C** Quantification of IBA1-labeled area in (**A**). n = 5 mice per group. **D** Western blots analysis of GFAP and IBA1 in the hippocampus lysates of WT mice and AD mice. **E** Quantitation of the levels of GFAP in (**D**). n = 5 mice per group. **F** Quantitation of the levels of IBA1 in (**D**). n = 5 mice per group. **G–I** The levels of inflammatory cytokines IL-6 (**G**), TNF-α (**H**) and IL-1β (**I**) in the hippocampus lysates of mice were measured by ELISA. For (**G–I**), data are pooled from three independent experiments. For (**B**, **C**, **E–I**), data are mean ± SEM, and a one-way ANOVA followed by Tukey's multiple comparison test was used for statistical analysis. *$P < 0.05$, **$P < 0.01$, ***$P < 0.001$, ****$P < 0.0001$, ns, not significant

Microglial DNase II deficiency induces neuroinflammation

Accumulation of DNA damage is known to stimulate an inflammatory response through innate immune signaling [36–38]. Consistently, significantly increased astrogliosis and microgliosis in the hippocampus of microglial DNase II-deficient WT and AD mice were observed by GFAP staining (Fig. 5A, B) and IBA1 staining (Fig. 5A, C), while the gliosis in 3xTg-KD mice were more severe. Western blots analysis also showed that the levels of GFAP (Fig. 5D, E) and IBA1 (Fig. 5D, F) were increased in the hippocampus lysates of microglial DNase II-deficient WT and AD mice. Moreover, the levels of inflammatory cytokines including IL-6 (Fig. 5G), TNF-α (Fig. 5H) and IL-1β (Fig. 5I) were higher in WT-KD and 3xTg-KD mice relative to their controls. Additionally, the levels of inflammatory cytokines including IL-6 (Fig. S6A), TNF-α (Fig.

S6B) and IL-1β (Fig. S6C) in the supernatant of primary microglia with DNase II knockdown were higher than that in the control. These results demonstrated that microglial DNase II deficiency caused an intense inflammatory response.

Microglial DNase II deficiency increases Aβ level and tauopathy

To examine the effect of microglial DNase II on AD pathogenesis, we detected the amyloid pathology and tauopathy in WT and AD mice treated with or without AAV-shDNase2a. The levels of Aβ42 and Aβ40 in insoluble hippocampal fractions of DNase II-deficient WT and AD mice were significantly increased (Fig. 6A, B). Immunostaining with anti-Aβ antibody 4G8 revealed the detectable increase of Aβ deposits in the hippocampal regions of microglial DNase II-deficient WT and AD mice relative to their controls (Fig. 6C, D). Western blots results indicated that microglial DNase II knockdown significantly increased the levels of PS1 and BACE1 in WT and AD mice, while the level of APP increased in 3xTg-KD mice but not in WT-KD mice (Fig. 6E–H). Moreover, increased levels of tau hyperphosphorylation detected by AT8 staining were observed in the hippocampal regions of microglial DNase II-deficient WT and AD mice (Fig. 6I, J). Consistently, microglial DNase II deficiency significantly increased p-tau levels in the brain lysates of WT and AD mice as detected by western blots (Fig. 6K, L). Tau and Aβ fibrillar are widely regarded as the pathogenic form of protein [39, 40]. We further determined the levels of fibrillar in mouse brain lysates by dot-blot using fibrillar specific antibody OC. Increased level of OC-positive fibrillar was observed in microglial DNase II-deficient WT and AD mice relative to their controls (Fig. 6M, N). Together, these results demonstrated that microglial DNase II deficiency increased Aβ level and tauopathy.

Microglial DNase II deficiency induces synapses loss

To explore the neuropathological mechanism in the memory loss of microglial DNase II deficient mice, the number of $NeuN^+$ neurons in hippocampus of WT and AD mice was measured. The number of $NeuN^+$ neurons was decreased in microglial DNase II deficient WT and AD mice (Fig. 7A, B). Moreover, the levels of postsynaptic density-95 (PSD95) and synaptophysin (SYN), and the number of intact synapses (indicated by co-localization of PSD95 and SYN) were significantly decreased in the brains of WT-KD mice and 3xTg-KD mice (Fig. 7C–F). These findings were confirmed by western blots analysis of PSD95 and SYN in the hippocampus lysates of WT and AD mice (Fig. 7G–I). The level of c-Fos also showed a decrease in the hippocampus lysates and neurons of WT and AD mice received AAV-shDNase2a injection, indicating that the survival and activity of neuron was reduced[41] (Fig. 7J–M). These results indicated that microglial DNase II deficiency induced neuronal damage and synapses loss.

Microglial DNase II deficiency actives complement pathway and promotes engulfment of synapses

During development, microglia play a crucial role in the refinement of neuronal circuits through the engulfment of excess synapses via a classical complement-dependent pathway [42]. Microglia have also been shown to excessively uptake synapses in a C3-dependent manner in AD models [43–46]. Stereotaxic AAV-shDNase2a injection resulted in elevated expression of multiple complement proteins, including C1q and C3 (Fig. 8A–C). The levels of $C3^+$ astrocytes significantly increased in microglial DNase II-deficient WT and AD mice (Fig. 8D, E), which were powerfully neurotoxicity and corelated with multiple neurodegenerative diseases especially AD [47, 48]. Moreover, we observed that PSD95 puncta engulfment was highly present in microglia in DNase II-deficient WT and AD mice (Fig. 8F, G), demonstrating that microglial DNase II deficiency promoted microglia engulfment of synapses.

(See figure on next page.)

Fig. 6 Microglial DNase II deficiency induces Aβ plaques and tau phosphorylation in WT and AD mice. **A**, **B** MSD analysis of Aβ42 (**A**) and Aβ40 (**B**) in the insoluble hippocampus lysates of WT mice and AD mice. n = 5 mice per group. **C** Representative images of $4G8^+$ Aβ plaques in hippocampus of WT mice and AD mice. Scale bars, 10 μm. **D** The area of $4G8^+$ Aβ plaque in hippocampus of mouse brains was quantified using ImageJ software. n = 5 mice per group. **E** Western blots analysis of APP, PS1 and BACE1 in the hippocampus lysates of WT mice and AD mice. **F–H** Quantitation of the levels of APP (**F**), PS1 (**G**) and BACE1 (**H**) in (**E**). n = 5 mice per group. **I** Detection of phosphorylated tau by immunolabeling AT8 in the hippocampal region of WT mice and AD mice. Scale bars, 10 μm. **J** Quantification of AT8-labeled area in (**I**). n = 5 mice per group. **K** Western blots analysis of AT8 in the hippocampus lysates of WT mice and AD mice. **L** Quantitation of the levels of AT8 in (**K**). n = 5 mice per group. **M** Dot-blot analysis of OC-positive fibrillar in the hippocampus lysates of WT mice and AD mice. **N** Quantification of OC-positive fibrillar in (M). n = 5 mice per group. For (**A**, **B**, **D**, **F–H**, **J**, **L**, **N**), data are mean ± SEM, and a one-way ANOVA followed by Tukey's multiple comparison test was used for statistical analysis. *$P < 0.05$, **$P < 0.01$, ***$P < 0.001$, ****$P < 0.0001$, ns, not significant

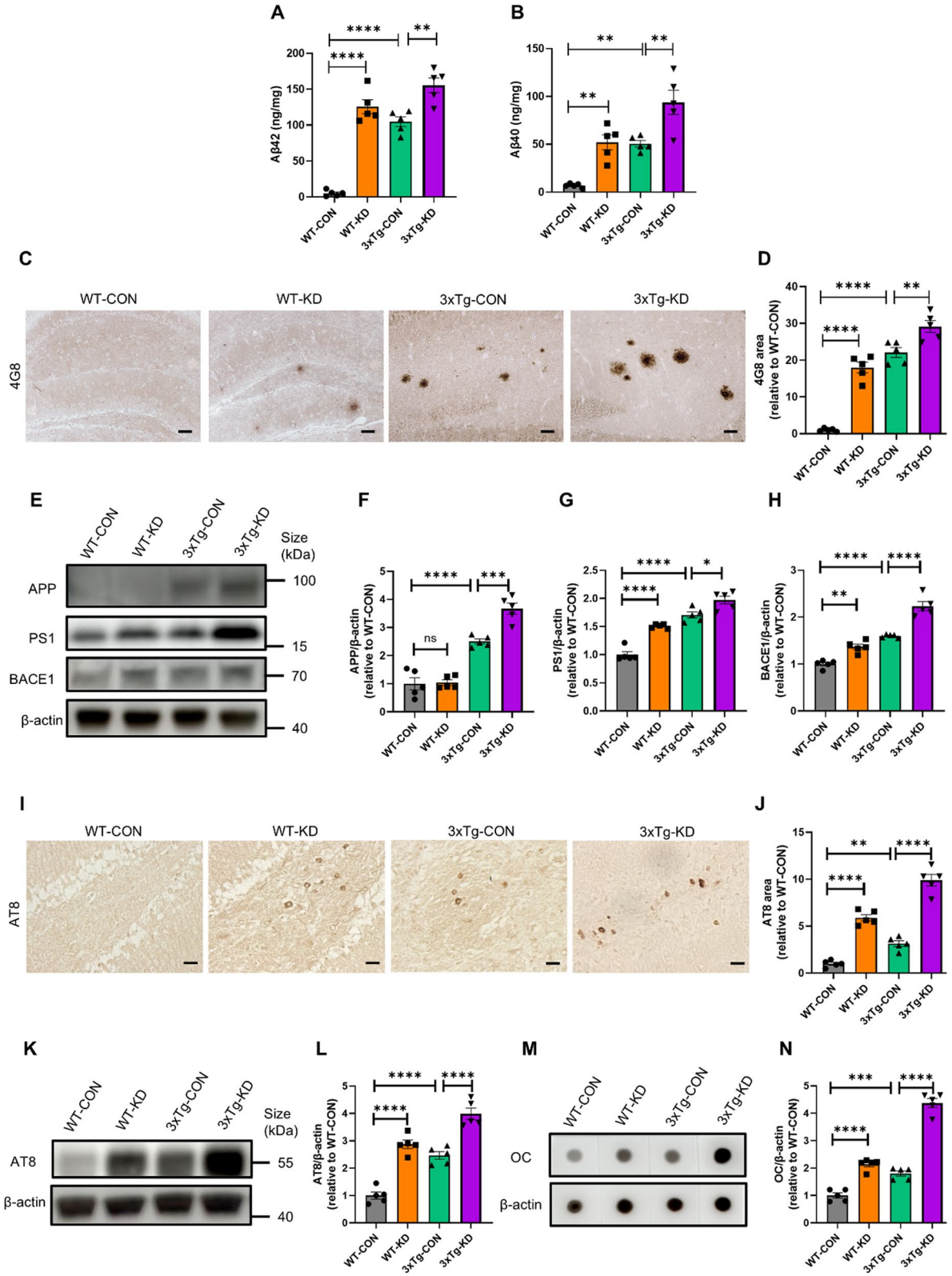

Fig. 6 (See legend on previous page.)

Discussion

DNase II plays a key role in maintain DNA homeostasis, which is downregulated in senescent cell and induces DNA accumulation in cytoplasm [17]. In the latest study, we have demonstrated that DNase II levels were decreased in the brains of aged WT mice, AD patients and AD mice, while neuronal DNase II deficiency induced tau hyperphosphorylation and neurodegeneration, which indicated that DNase II may be a risk factor of AD [18]. However, the effect of microglial DNase II on AD neuropathology has not been reported. In present study, we showed that the levels of microglial DNase II were downregulated in the brains of 3xTg-AD mice. Microglial DNase II deficiency resulted in activating of the cGAS-STING and IFN-I pathway and inducing the alternation of microglial transcriptional signatures and morphology, initiating neuroinflammation, leading to complement pathway activation and synapse loss, increasing Aβ load and tauopathy and ultimately inducing cognitive impairment.

Neuronal DNase II knockdown mainly drove tau hyperphosphorylation, microglia DNase II knockdown mainly promoted neuroinflammation, and the decrease of DNase II level in these cells jointly led to the pathological process of AD.

Chronic activation of innate immunity is a trigger for neuroinflammation, which is critically biological process in the progression of AD. Many evident for activation of the IFN pathway in human AD tissues, specifically type I IFN pathway, suggest that IFN-I in mediating neuroinflammation and neuropathology in AD models [26, 27, 29]. Recently studies have identified the activation of the cGAS-STING pathway induced by cytoplasmic dsDNA, accelerates AD progression [25, 28]. The presence of cGAS-STING and IFN-I signature in brain cells, particular in microglia, is increasingly being associated with aging and neurodegenerative disease in various species [49–53]. However, it is remaining unclear what factors cause microglia to activate the cGAS-STING and IFN-I pathways. Our analysis revealed that microglial DNase II downregulation induced DNA accumulation in cytoplasm, and resulted in the activation of the cGAS-STING and IFN-I pathway in WT mice and primary microglia. Notably, these pathways were markedly hyperactivated in 3xTg-KD mice, maybe caused by lower microglial DNase II levels in AD mice. Our results demonstrated potent effects of DNase II on activating microglial by inducing morphological changes and transcriptional signatures changes, expression of proinflammatory factors, and signaling molecules.

In this study, we found the microglial DNase II deficiency increased of Aβ levels and phosphorylated tau in the brain of mice, with exacerbation by Aβ and tauopathy. Microglial IFN-I response universally accompanies brain amyloidosis and tauopathy in vivo [26, 29], a proteome analysis revealed that IFN-I pathway is activated early and persists in microglia of murine Aβ models [54]. Microglia are chronically overactivated by accumulated Aβ during AD pathogenesis and can trigger prominent neurotoxicity in the CNS through secreting proinflammatory factors such as IL-1β, IL-6, and TNF-α. These inflammatory cytokines can not only promote Aβ production, but also reciprocally facilitate microglial response to Aβ, thereby forming a vicious cycle between Aβ-induced pathogenesis and microglia-mediated neuroinflammation [55, 56]. Previous study shown that spatial propagation of microglial activation and tau accumulation colocalized in a Braak-like pattern in the living human brain [57]. In this study, we demonstrated that microglial DNase II deficiency induced microglial activation, secreting proinflammatory factors and IFN-I pathway activation which may induce AD-like pathology (Aβ accumulation and tau hyperphosphorylation).

Within brain cells, neurons are susceptible to the toxicity of the neurodegenerative proteins such as Aβ and hyperphosphorylated tau, which causes a harmful stress to adversely affect multiple cellular biological functions, such as reducing the survival and activity of neurons. Synapse loss is clinically associated with cognitive decline in AD [58, 59]. In this study, we found that microglial

(See figure on next page.)

Fig. 7 Microglial DNase II deficiency induces synapses loss in WT and AD mice. **A** Immunolabeling of NeuN (green) in the brains of WT mice and AD mice. Scale bars, 5 μm. **B** Quantification number of NeuN positive cells in (**A**). n = 5 mice per group. **C** Immunolabeling of PSD95 (red) and synaptophysin (SYN) (green) puncta in the brains of WT mice and AD mice. Co-localized PSD95 and SYN puncta are indicated by circles. Scale bars, 5 μm. **D** Quantification of PSD95 puncta in (**C**). n = 5 mice per group. **E** Quantification of SYN puncta in (**C**). n = 5 mice per group. **F** Quantification of co-localized PSD95 and SYN puncta in (**C**). n = 5 mice per group. **G** Western blots analysis of PSD95 and SYN in the hippocampal homogenates of WT mice and AD mice. **H** Quantitation of the levels of PSD95 in the brains of mice in (**G**). n = 5 mice per group. **I** Quantitation of the levels of SYN in the brains of mice in (**G**). n = 5 mice per group. **J** Western blots analysis of c-FOS in the hippocampal homogenates of WT mice and AD mice. **K** Quantitation of the levels of c-FOS in the hippocampal homogenates of mice in (**J**). n = 5 mice per group. **L** Representative images of c-Fos (red) and DAPI (blue) fluorescence staining in the $MAP2^+$ (green) neurons of WT mice and AD mice. Scale bars, 10 μm. **M** Quantification of c-Fos fluorescent area in (L). n = 5 mice per group. For (**B**, **D–F**, **H–I**, **K**, **M**), data are mean ± SEM, and a one-way ANOVA followed by Tukey's multiple comparison test was used for statistical analysis. *$P < 0.05$, **$P < 0.01$, ***$P < 0.001$, ****$P < 0.0001$, ns, not significant

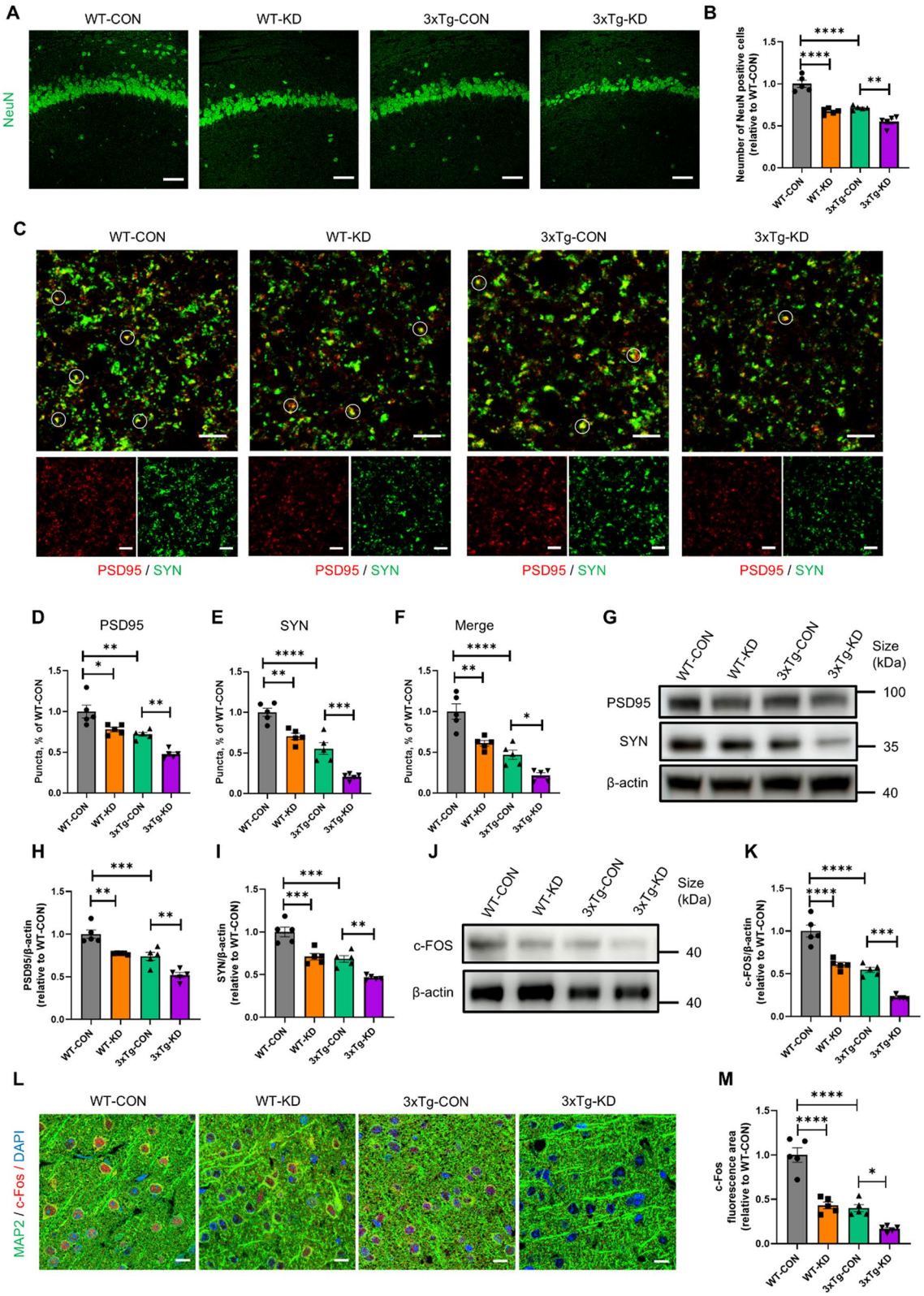

Fig. 7 (See legend on previous page.)

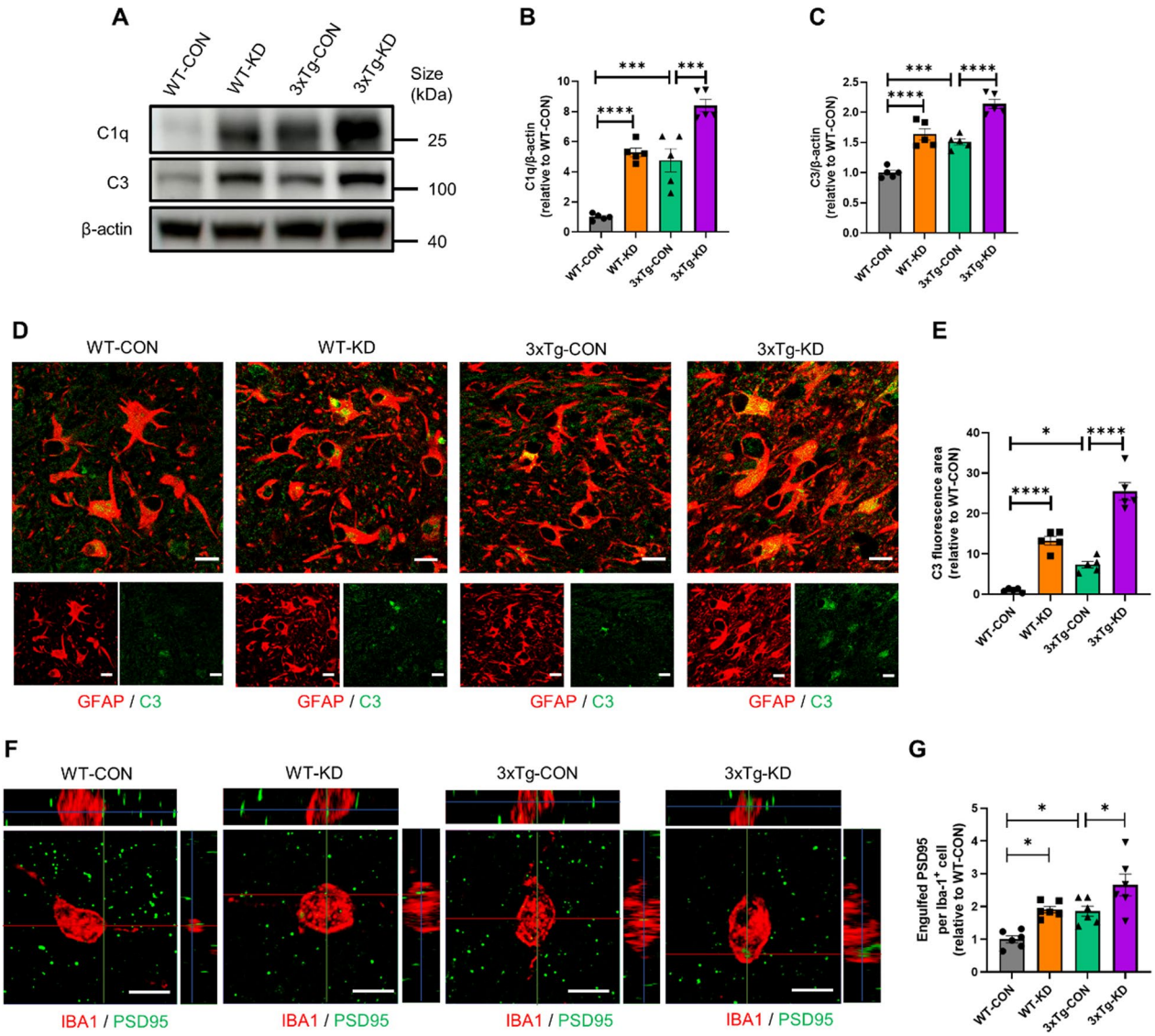

Fig. 8 Microglial DNase II deficiency actives complement pathway and induces engulfment of synapses. **A** Western blots analysis of C1q and C3 in the hippocampal homogenates of WT mice and AD mice. **B** Quantitation of the levels of C1q in the hippocampal homogenates of mice in (**A**). n = 5 mice per group. **C** Quantitation of the levels of C3 in the hippocampal homogenates of mice in (**A**). n = 5 mice per group. **D** Representative images of C3 (green) and GFAP (red) fluorescence staining in the hippocampus of WT mice and AD mice. Scale bars, 10 μm. **E** Quantification of C3 fluorescent area in (**D**). n = 5 mice per group. **F** Representative images show the engulfed PSD95 (red) puncta within IBA1$^+$ (green) microglial cells in the brains of WT mice and AD mice, Scale bars, 5 μm. **G** Quantification of PSD95 puncta per IBA1$^+$ microglial cell. n = 6 mice per group. For (**B**, **C**, **E**, **G**), data are mean ± SEM, and a one-way ANOVA followed by Tukey's multiple comparison test was used for statistical analysis. *$P < 0.05$, **$P < 0.01$, ***$P < 0.001$, ****$P < 0.0001$, ns, not significant

DNase II deficiency induced cognitive impairment, which may be due to numbers of synapses loss. The profound activation of the IFN-I pathway in MGnD microglia supports that the microglia participates in neuropathology via complement and IFN-mediated synapse elimination [26]. Our study provides a major advance in the mechanistic understanding of this pathogenic process by identifying an axis that connects DNase II, complement, and synapse loss. We have shown that microglial DNase II regulated the expression of multiple components of the complement cascade and mediated microglial synapse elimination, while the lower DNase II levels in 3xTg-KD mice caused higher complement proteins levels and more synapse engulfment in microglia.

In conclusion, we here identified the effect of microglial DNase II on the development of AD neuropathology, and found that microglial DNase II deficiency significantly induced the alternation of microglial

transcriptional signatures and morphology, initiated neuroinflammation, Aβ load and tauopathy, led to synapse loss and cognitive impairment. Our study demonstrated that DNase II, as a new risk factors for AD development, may be a potential target of AD.

Abbreviations

AD	Alzheimer's disease
Aβ	β-Amyloid
cGAS	Cyclic GMP-AMP synthase
CNS	Central nervous system
DAB	Diaminobenzidine
DNase II	Deoxyribonuclease 2
dsDNA	Double stranded DNA
GFAP	Glial fibrillary acidic protein
IBA1	Ionized calcium-binding adapter molecule 1
IL-1β	Interleukin-1β
IL-6	Interleukin 6
IRF3	Interferon regulatory factor 3
MWM	Morris water maze
NOR	Novel objection recognition
PSD95	Postsynaptic density protein-95
SASP	Senescence-associated secretory phenotype
STING	Stimulator of interferon genes protein
SYN	Synaptophysin
TBK1	TANK-binding kinase 1
TNF-α	Tumor necrosis factor α
IFN-I	Type-I-interferon

Supplementary Information

The online version contains supplementary material available at https://doi.org/10.1186/s12974-025-03333-6.

Additional file 1.

Acknowledgements
We would like to thank the caretakers from the Laboratory Animal resources Center of Tsinghua University, for their contribution in maintaining the mouse colonies, specifically the weighing and feeding of the mice.

Author contributions
R.-T.L. designed the experiments; L.-J.L., X.-Y.S., performed immunohistochemistry, L.-J.L., S.-Y.L. performed animal experiments, ELISA and Dot-blot; L.-J.L., S.-Y.L., J.Z., Y.-R.H., and. X.-Y.N. conducted the Western blots experiments and q-PCR; Y.-R.H. provided samples and advice; L.-J.L., S.-Y.L., X.-Y.D. analyzed the data; L.-J.L., and R.-T.L. wrote the manuscript. All authors have read and approved the article.

Funding
This work was supported by funding from the Strategic Priority Research Program of the Chinese Academy of Sciences (XDB39050600), the National Natural Science Foundation of China (82150107, 81971073 and 82401674), and the National Key Research and Development Program of China (no. 2020YFA0712402).

Data Availability
No datasets were generated or analysed during the current study.

Declarations

Ethics approval and consent to participate
All animal experiments were performed in accordance with the China Public Health Service Guide for the Care and Use of Laboratory Animals. Experiments involving mice and protocols were approved by the Institutional Animal Care and Use Committee of Tsinghua University. Authors are responsible for correctness of the statements provided in the manuscript.

Consent for publication
All authors have reviewed the final manuscript and consent to publication.

Competing interests
The authors declare no competing interests.

Author details
[1]State Key Laboratory of Biopharmaceutical Preparation and Delivery, Institute of Process Engineering, Chinese Academy of Sciences, Haidian District, Beijing 100190, China. [2]University of Chinese Academy of Sciences, Beijing 100049, China. [3]College of Life Science, Ningxia University, Yinchuan 750021, China.

Received: 7 November 2024 Accepted: 2 January 2025
Published: 20 January 2025

References

1. (2023) 2023 Alzheimer's disease facts and figures. Alzheimer Dement 19:1598–1695
2. Jack CR, Bennett DA, Blennow K, Carrillo MC, Dunn B, Haeberlein SB, Holtzman DM, Jagust W, Jessen F, Karlawish J, et al. NIA-AA Research Framework: Toward a biological definition of Alzheimer's disease. Alzheimers Dement. 2018;14:535–62.
3. Heppner FL, Ransohoff RM, Becher B. Immune attack: the role of inflammation in Alzheimer disease. Nat Rev Neurosci. 2015;16:358–72.
4. Perlmutter D. Preventing Alzheimer's disease. J Am Coll Nutr. 2016;35:732–3.
5. Du L, Zhang Y, Chen Y, Zhu J, Yang Y, Zhang HL. Role of microglia in neurological disorders and their potentials as a therapeutic target. Mol Neurobiol. 2017;54:7567–84.
6. Lehnardt S. Innate immunity and neuroinflammation in the CNS: The role of microglia in Toll-like receptor-mediated neuronal injury. Glia. 2010;58:253–63.
7. Hansen DV, Hanson JE, Sheng M. Microglia in Alzheimer's disease. J Cell Biol. 2018;217:459–72.
8. Salter MW, Stevens B. Microglia emerge as central players in brain disease. Nat Med. 2017;23:1018–27.
9. Gao C, Jiang J, Tan Y, Chen S. Microglia in neurodegenerative diseases: mechanism and potential therapeutic targets. Signal Transduct Target Ther. 2023;8:359.
10. Leng F, Edison P. Neuroinflammation and microglial activation in Alzheimer disease: Where do we go from here? Nat Rev Neurol. 2021;17:157–72.
11. Kwon HS, Koh SH. Neuroinflammation in neurodegenerative disorders: The roles of microglia and astrocytes. Transl Neurodegener. 2020;9:42.
12. Evans CJ, Aguilera RJ. DNase II: genes, enzymes and function. Gene. 2003;322:1–15.
13. Lan YY, Londono D, Bouley R, Rooney MS, Hacohen N. Dnase2a deficiency uncovers lysosomal clearance of damaged nuclear DNA via autophagy. Cell Rep. 2014;9:180–92.
14. Chan MP, Onji M, Fukui R, Kawane K, Shibata T, Saitoh S-I, Ohto U, Shimizu T, Barber GN, Miyake K. DNase II-dependent DNA digestion is required for DNA sensing by TLR9. Nat Commun. 2015;6:5853.
15. Matsui H, Ito J, Matsui N, Uechi T, Onodera O, Kakita A. Cytosolic dsDNA of mitochondrial origin induces cytotoxicity and neurodegeneration in cellular and zebrafish models of Parkinson's disease. Nat Commun. 2021;12:3101.
16. Oka T, Hikoso S, Yamaguchi O, Taneike M, Takeda T, Tamai T, Oyabu J, Murakawa T, Nakayama H, Nishida K, et al. Mitochondrial DNA that escapes from autophagy causes inflammation and heart failure. Nature. 2012;485:251–5.
17. Takahashi A, Loo TM, Okada R, Kamachi F, Watanabe Y, Wakita M, Watanabe S, Kawamoto S, Miyata K, Barber GN, et al. Downregulation of cytoplasmic DNases is implicated in cytoplasmic DNA accumulation and SASP in senescent cells. Nat Commun. 2018;9:1249.
18. Li LJ, Sun XY, Huang YR, Lu S, Xu YM, Yang J, Xie XX, Zhu J, Niu XY, Wang D, et al. Neuronal double-stranded DNA accumulation induced by DNase II deficiency drives tau phosphorylation and neurodegeneration. Transl Neurodegener. 2024;13:39.

19. Ablasser A, Chen ZJ. cGAS in action: Expanding roles in immunity and inflammation. Science. 2019;363:eaat8657.
20. Li Q, Cao Y, Dang C, Han B, Han R, Ma H, Hao J, Wang L. Inhibition of double-strand DNA-sensing cGAS ameliorates brain injury after ischemic stroke. EMBO Mol Med. 2020;12: e11002.
21. Sliter DA, Martinez J, Hao L, Chen X, Sun N, Fischer TD, Burman JL, Li Y, Zhang Z, Narendra DP, et al. Parkin and PINK1 mitigate STING-induced inflammation. Nature. 2018;561:258–62.
22. Sharma M, Rajendrarao S, Shahani N, Ramirez-Jarquin UN, Subramaniam S. Cyclic GMP-AMP synthase promotes the inflammatory and autophagy responses in Huntington disease. Proc Natl Acad Sci U S A. 2020;117:15989–99.
23. Yu CH, Davidson S, Harapas CR, Hilton JB, Mlodzianoski MJ, Laohamonthonkul P, Louis C, Low RRJ, Moecking J, De Nardo D, et al. TDP-43 triggers mitochondrial DNA release via mPTP to activate cGAS/STING in ALS. Cell. 2020;183:636–49.
24. Jin M, Shiwaku H, Tanaka H, Obita T, Ohuchi S, Yoshioka Y, Jin X, Kondo K, Fujita K, Homma H, et al. Tau activates microglia via the PQBP1-cGAS-STING pathway to promote brain inflammation. Nat Commun. 2021;12:6565.
25. Xie X, Ma G, Li X, Zhao J, Zhao Z, Zeng J. Activation of innate immune cGAS-STING pathway contributes to Alzheimer's pathogenesis in 5xFAD mice. Nat Aging. 2023;3:202–12.
26. Roy ER, Wang B, Wan YW, Chiu G, Cole A, Yin Z, Propson NE, Xu Y, Jankowsky JL, Liu Z, et al. Type I interferon response drives neuroinflammation and synapse loss in Alzheimer disease. J Clin Invest. 2020;130:1912–30.
27. Roy ER, Chiu G, Li S, Propson NE, Kanchi R, Wang B, Coarfa C, Zheng H, Cao W. Concerted type I interferon signaling in microglia and neural cells promotes memory impairment associated with amyloid beta plaques. Immunity. 2022;55:879–94.
28. Gulen MF, Samson N, Keller A, Schwabenland M, Liu C, Gluck S, Thacker VV, Favre L, Mangeat B, Kroese LJ, et al. cGAS-STING drives ageing-related inflammation and neurodegeneration. Nature. 2023;620:374–80.
29. Jin M, Xu R, Wang L, Alam MM, Ma Z, Zhu S, Martini AC, Jadali A, Bernabucci M, Xie P, et al. Type-I-interferon signaling drives microglial dysfunction and senescence in human iPSC models of Down syndrome and Alzheimer's disease. Cell Stem Cell. 2022;29:1135–53.
30. Wheeler MA, Jaronen M, Covacu R, Zandee SEJ, Scalisi G, Rothhammer V, Tjon EC, Chao CC, Kenison JE, Blain M, et al. Environmental control of astrocyte pathogenic activities in CNS inflammation. Cell. 2019;176:581–96.
31. Sun XY, Li LJ, Dong QX, Zhu J, Huang YR, Hou SJ, Yu XL, Liu RT. Rutin prevents tau pathology and neuroinflammation in a mouse model of Alzheimer's disease. J Neuroinflammation. 2021;18:131.
32. Li T, Chen ZJ. The cGAS-cGAMP-STING pathway connects DNA damage to inflammation, senescence, and cancer. J Exp Med. 2018;215:1287–99.
33. Cheon H, Stark GR. Unphosphorylated STAT1 prolongs the expression of interferon-induced immune regulatory genes. Proc Natl Acad Sci U S A. 2009;106:9373–8.
34. Ikushima H, Negishi H, Taniguchi T. The IRF family transcription factors at the interface of innate and adaptive immune responses. Cold Spring Harb Symp Quant Biol. 2013;78:105–16.
35. Honda K, Yanai H, Negishi H, Asagiri M, Sato M, Mizutani T, Shimada N, Ohba Y, Takaoka A, Yoshida N, Taniguchi T. IRF-7 is the master regulator of type-I interferon-dependent immune responses. Nature. 2005;434:772–7.
36. Nakad R, Schumacher B. DNA damage response and immune defense: links and mechanisms. Front Genet. 2016;7:147.
37. Nastasi C, Mannarino L, D'Incalci M. DNA damage response and immune defense. Int J Mol Sci. 2020;21:7504.
38. Xu Y. DNA damage: a trigger of innate immunity but a requirement for adaptive immune homeostasis. Nat Rev Immunol. 2006;6:261–70.
39. Shafiei SS, Guerrero-Munoz MJ, Castillo-Carranza DL. Tau oligomers: cytotoxicity, propagation, and mitochondrial damage. Front Aging Neurosci. 2017;9:83.
40. Huang YR, Liu RT. The toxicity and polymorphism of beta-amyloid oligomers. Int J Mol Sci. 2020;21:4477.
41. Tunc-Ozcan E, Peng CY, Zhu Y, Dunlop SR, Contractor A, Kessler JA. Activating newborn neurons suppresses depression and anxiety-like behaviors. Nat Commun. 2019;10:3768.
42. Schafer DP, Lehrman EK, Kautzman AG, Koyama R, Mardinly AR, Yamasaki R, Ransohoff RM, Greenberg ME, Barres BA, Stevens B. Microglia sculpt postnatal neural circuits in an activity and complement-dependent manner. Neuron. 2012;74:691–705.
43. Hong S, Beja-Glasser VF, Nfonoyim BM, Frouin A, Li S, Ramakrishnan S, Merry KM, Shi Q, Rosenthal A, Barres BA, et al. Complement and microglia mediate early synapse loss in Alzheimer mouse models. Science. 2016;352:712–6.
44. Bartels T, De Schepper S, Hong S. Microglia modulate neurodegeneration in Alzheimer's and Parkinson's diseases. Science. 2020;370:66–9.
45. Rajendran L, Paolicelli RC. Microglia-mediated synapse loss in Alzheimer's disease. J Neurosci. 2018;38:2911–9.
46. Shi Q, Chowdhury S, Ma R, Le KX, Hong S, Caldarone BJ, Stevens B, Lemere CA. Complement C3 deficiency protects against neurodegeneration in aged plaque-rich APP/PS1 mice. Sci Transl Med. 2017;9:eaaf6295.
47. Lawrence JM, Schardien K, Wigdahl B, Nonnemacher MR. Roles of neuropathology-associated reactive astrocytes: a systematic review. Acta Neuropathol Commun. 2023;11:42.
48. Liddelow SA, Guttenplan KA, Clarke LE, Bennett FC, Bohlen CJ, Schirmer L, Bennett ML, Munch AE, Chung WS, Peterson TC, et al. Neurotoxic reactive astrocytes are induced by activated microglia. Nature. 2017;541:481–7.
49. Baruch K, Deczkowska A, David E, Castellano JM, Miller O, Kertser A, Berkutzki T, Barnett-Itzhaki Z, Bezalel D, Wyss-Coray T, et al. Aging. Aging-induced type I interferon response at the choroid plexus negatively affects brain function. Science. 2014;346:89–93.
50. Tabula Muris C. A single-cell transcriptomic atlas characterizes ageing tissues in the mouse. Nature. 2020;583:590–5.
51. Friedman BA, Srinivasan K, Ayalon G, Meilandt WJ, Lin H, Huntley MA, Cao Y, Lee SH, Haddick PCG, Ngu H, et al. Diverse brain myeloid expression profiles reveal distinct microglial activation states and aspects of Alzheimer's disease not evident in mouse models. Cell Rep. 2018;22:832–47.
52. Deczkowska A, Matcovitch-Natan O, Tsitsou-Kampeli A, Ben-Hamo S, Dvir-Szternfeld R, Spinrad A, Singer O, David E, Winter DR, Smith LK, et al. Mef2C restrains microglial inflammatory response and is lost in brain ageing in an IFN-I-dependent manner. Nat Commun. 2017;8:717.
53. Holtman IR, Raj DD, Miller JA, Schaafsma W, Yin Z, Brouwer N, Wes PD, Moller T, Orre M, Kamphuis W, et al. Induction of a common microglia gene expression signature by aging and neurodegenerative conditions: a co-expression meta-analysis. Acta Neuropathol Commun. 2015;3:31.
54. Sebastian Monasor L, Muller SA, Colombo AV, Tanrioever G, Konig J, Roth S, Liesz A, Berghofer A, Piechotta A, Prestel M, et al. Fibrillar Abeta triggers microglial proteome alterations and dysfunction in Alzheimer mouse models. Elife. 2020;9: e54083.
55. Goldgaber D, Harris HW, Hla T, Maciag T, Donnelly RJ, Jacobsen JS, Vitek MP, Gajdusek DC. Interleukin 1 regulates synthesis of amyloid beta-protein precursor mRNA in human endothelial cells. Proc Natl Acad Sci U S A. 1989;86:7606–10.
56. Cai Z, Hussain MD, Yan LJ. Microglia, neuroinflammation, and beta-amyloid protein in Alzheimer's disease. Int J Neurosci. 2014;124:307–21.
57. Pascoal TA, Benedet AL, Ashton NJ, Kang MS, Therriault J, Chamoun M, Savard M, Lussier FZ, Tissot C, Karikari TK, et al. Microglial activation and tau propagate jointly across Braak stages. Nat Med. 2021;27:1592–9.
58. Scheff SW, DeKosky ST, Price DA. Quantitative assessment of cortical synaptic density in Alzheimer's disease. Neurobiol Aging. 1990;11:29–37.
59. Terry RD, Masliah E, Salmon DP, Butters N, DeTeresa R, Hill R, Hansen LA, Katzman R. Physical basis of cognitive alterations in Alzheimer's disease: synapse loss is the major correlate of cognitive impairment. Ann Neurol. 1991;30:572–80.

Publisher's Note